Check for updates

ADVANCED MATERIALS TECHNOLOGIES
www.advmattechnol.de

Fully Screen-Printed, Flexible, and Scalable Organic Monolithic Thermoelectric Generators

Irene Brunetti, Federico Ferrari, Nathan James Pataki, Sina Abdolhosseinzadeh, Jakob Heier, L. Jan Anton Koster, Ulrich Lemmer, Martijn Kemerink, and Mario Caironi**

Energy-harvesting technologies offer a sustainable, maintenance-free alternative to conventional energy-storage solutions in distributed low-power applications. Flexible thermoelectric generators (TEGs) can generate electric power from a temperature gradient, even on complex surfaces. Organic materials are ideal candidates for flexible TEGs due to their good solution-processability, natural abundance, low weight, and flexibility. Electronic and thermoelectric properties of organic materials have steadily progressed, while device architectures leveraging their advantages are largely missing. Here, a design and fabrication method are proposed for producing fully screen-printed, flexible monolithic organic TEGs scalable up to m^2, compatible with any screen-printable ink. This approach is validated, along with its scalability, by printing TEGs composed of two different active inks, in three configurations, with up to 800 thermoelements, with performances well matching simulations based on materials parameters. It is demonstrated that by using an additive-free graphene ink, a remarkable power density of 15 nW cm^{-2} at $\Delta T =$ 29.5 K can be achieved, with an estimated weight-normalized power output of 1 µW g^{-1}, highlighting a strong potential in portability. Owing to such power density, only limited areas are required to generate microwatts, sufficient for operating low-power electronic devices such as sensors, and wearables.

1. Introduction

In recent years, the escalating global energy demand has catalysed extensive research into innovative energy sources, with a marked emphasis on renewables.[1,2] Advances in low-power electronic components, specifically sensors and microelectronics within the domain of the Internet of Things (IoT), have led to a substantial reduction in power requirements for applications, now reaching the microwatt range.[3] This reduction in power consumption has facilitated the utilization of diverse energy harvesting sources across various use cases, including wearables, smart industry applications and smart grid monitoring.[4–6]

Among these alternative energy sources, low-grade thermal energy harvesting is gaining recognition as a viable and sustainable option.[7] Thermoelectric generators (TEGs), capable of directly converting thermal energy into electrical energy, offer significant promise for powering distributed nodes in the IoT in a sustainable way.[8,9] Traditionally, inorganic semiconductors and their alloys such as Sb_2Te_3, Bi_2Te_3, and PbTe have been the predominant materials in commercial thermoelectric applications.[10] However, these materials are not without limitations, including high cost-per-watt,[11] scarcity, toxicity, and the requirement for energy-intensive processing.[12,13]

In contrast, organic thermoelectric materials offer a non-toxic, earth-abundant alternative,[14] and, additionally, enable the development of more lightweight and flexible TEGs. Moreover,

I. Brunetti, U. Lemmer
InnovationLab
Speyererstr. 4, 69115 Heidelberg, Germany
E-mail: irene.brunetti@innovationlab.de
I. Brunetti, U. Lemmer
Light Technology Institute
Karlsruhe Institute of Technology Engesserstrasse 13
76131 Karlsruhe, Germany

The ORCID identification number(s) for the author(s) of this article can be found under https://doi.org/10.1002/admt.202302058

© 2024 The Authors. Advanced Materials Technologies published by Wiley-VCH GmbH. This is an open access article under the terms of the Creative Commons Attribution License, which permits use, distribution and reproduction in any medium, provided the original work is properly cited.

DOI: 10.1002/admt.202302058

F. Ferrari, L. J. A. Koster
Zernike Institute for Advanced Materials
University of Groningen Nijenborgh 4
Groningen 9747 AG, The Netherlands
N. J. Pataki, M. Caironi
Center for Nano Science and Technology
Istituto Italiano di Tecnologia Via Rubattino 81
Milano 20134, Italy
E-mail: mario.caironi@iit.it
N. J. Pataki
Department of Physic
Politecnico di Milano
Piazza Leonardo da Vinci 32, Milano 20133, Italy
S. Abdolhosseinzadeh, J. Heier
Laboratory for Functional Polymers
Swiss Federal Laboratories for Materials Science and Technology (Empa)
Überlandstrasse 129
Dübendorf CH-8600, Switzerland

Table 1. Number of thermocouples integrated in a fully printed organic TEGs, along with the corresponding printing technique used.

References	Number of thermocouples	Printing technique
[31]	10	3D print
[32]	6	Dispenser print
[33]	60	Drop cast
[34]	4	Inkjet print
[35]	20	Inkjet print
[18]	1	3D print
[36]	9	Spray coat
This work	800	Screen print

traditional inorganic TEGs often involve capital-intensive and environmentally impactful manufacturing techniques.[12,13] Instead, solution-processible, organic materials compatible with large-area printing techniques present a more cost-effective and sustainable manufacturing alternative.[15] These printing techniques, such as 3D printing, inkjet printing, screen printing and roll-to-roll printing, facilitate the scalability of TEG production, thereby reducing the time and cost of production.[16,17]

However, to date, only a few works in the field of organic thermoelectrics have presented studies on architectures and fabrication methods of truly scalable printed devices.[18–23] The majority of organic TEGs presented in the literature primarily focus on exhibiting the thermoelectric properties of organic materials by fabricating simple, proof-of-concept TEGs with approaches that are unsuitable for scaling.[24,25] These proof-of-concept devices usually exhibit power outputs significantly below the expected performance based on the figures of merit (zT) of the constituent materials. Furthermore, the majority of high-density organic TEGs are limited to small-area devices ($A_{TEG} << cm^2$), due to the limited scalability of the fabrication techniques, and demonstrate a low absolute power output.[26–29] So far, the reported fully printed organic TEGs presented a limited number of thermocouples, up to a maximum of 60 (**Table 1**).

This work presents a scalable methodology for TEG fabrication utilizing an entirely screen-printing process while demonstrating the reliability and adaptability of the fabrication method. The devices presented are the first large-area, fully printed TEGs with a structure that can be easily scaled up to m^2-areas. By exploiting a recently reported additive-free graphene ink,[30] a fully screen-printed 1×1 cm^2 TEG is demonstrated. The graphene-based TEG exhibits a power output of 15 nW at $\Delta T = 29.5$ K, in good agreement with numerical simulations and expectations based on the zTs of the constituent materials. Following the initial 1×1 cm^2 demonstration, the architecture was scaled up to 10×10 cm^2 devices consisting of 800 thermocouples.

The fully printed TEG architecture not only meets the power requirements of low-power sensors and IoT devices but also demonstrates the scalability and versatility of the fabrication method that can produce improved TEGs when more efficient inks are developed. Importantly, the TEG fabrication process is executed using an industrial-scale manufacturing process under ambient conditions, enabling the concurrent printing of multiple TEGs. This substantially reduces both production time and expense, representing a significant step forward in the development of organic TEGs.

2. Results and Discussion

2.1. Design of the TEG Structure

In the construction of the TEG, a vertical configuration was selected to maximize the number of thermocouples per unit of area, thereby increasing the power density and favoring good thermal contact with the heat source and sink. The design adopted is based on the Π-shape structure, where the legs of the devices are positioned perpendicular to the heat flow.[37] This architecture was replicated using an exclusively screen-printed fabrication process (**Figure 1a**), resulting in a monolithic thermoelectric generator. Given the limited availability of air-stable, screen-printable organic n-type materials,[38] an organic unipolar TEG was produced by replacing the n-type legs in a typical Π-shape structure with conductive Ag interconnections.

The screen-printing process for fabricating the TEG structure involves the deposition of five distinct layers, as shown in Figure 1b–d. Each layer is defined by a different screen with a different mesh layout that allows the ink to pass only through a defined area. A silver bottom contact layer (3 µm thick), required to interconnect the thermocouples, was first screen-printed onto a flexible, 25 µm thin Kapton polyimide substrate (Figure 1b), followed by an insulating layer (15 µm) with circular wells corresponding to each leg (Figure 1c). The wells were filled by screen-printing the p-type material to define the p-legs (Figure 1d), followed by a silver material to define the interconnecting legs (Figure 1e). Last, silver contacts (3 µm) were screen-printed to complete the TEG (Figure 1f). The geometrical fill factor (FF) of the TEG architecture, an important design parameter representing the ratio of the area covered by the thermoelectric materials to the total device area,[39] was determined to be 0.28. For devices with interconnecting silver legs, FF is effectively halved ($FF = 0.14$) since the silver does not contribute to the power output.

The exact dimensions of the layout are reported in the Supporting Information (Figure S1, Supporting Information). Additionally, a thin film of parylene (1 µm) was deposited as a final step to provide electrical insulation to the TEGs. Employing this methodology, TEGs comprising of $n = 4$, $n = 8$, and $n = 800$ vertical thermocouples with areas of 0.5 cm^2, 1 cm^2 and 100 cm^2 respectively, were fabricated.

2.2. Validation of the TEG Architecture and Fabrication Process

The design of the TEG architecture and the described fabrication methodology were initially validated using a screen-printable

M. Kemerink
Institute for Molecular Systems Engineering and Advanced Materials
Heidelberg University
69120 Heidelberg, Germany

© 2024 The Authors. Advanced Materials Technologies published by Wiley-VCH GmbH

2365709x, 0, Downloaded from https://onlinelibrary.wiley.com/doi/10.1002/admt.202302058 by Karlsruher Institut F., Wiley Online Library on [10/04/2024]. See the Terms and Conditions (https://onlinelibrary.wiley.com/terms-and-conditions) on Wiley Online Library for rules of use; OA articles are governed by the applicable Creative Commons License

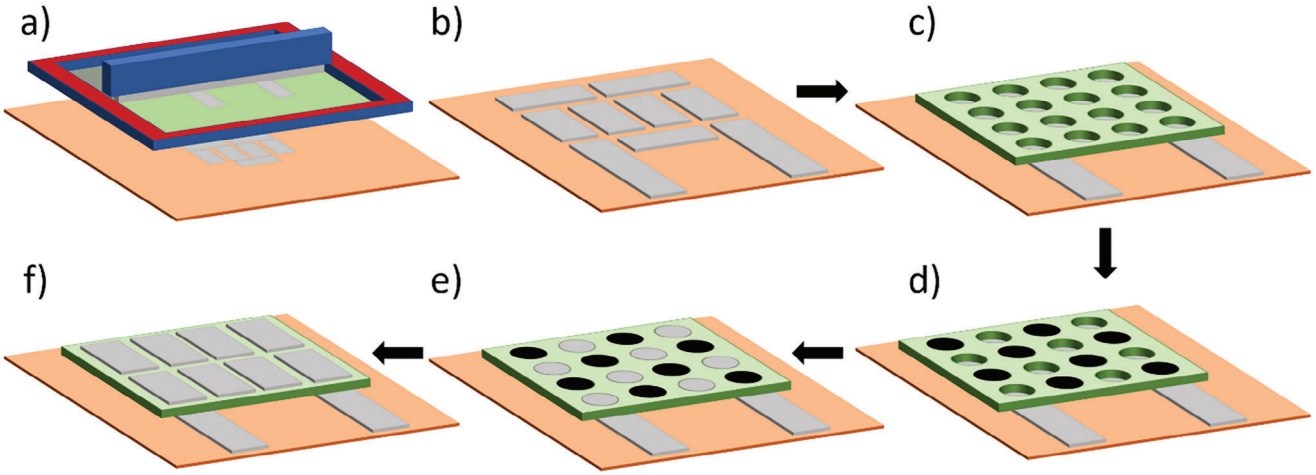

Figure 1. a) sketch drawing of the screen-printed technique. b) printed bottom silver contact layer c) printed insulator layer d) printed p-type material (Graphene, PEDOT:PSS) legs layer. e) printed silver legs layer. f) printed top silver contact layer.

formulation (Clevios SV4, Heraeus) of a widely used p-type organic thermoelectric material, poly(3,4-ethylenedioxythiophene) polystyrene sulfonate (PEDOT:PSS), to print the p-type legs, while a commercially available screen-printable Ag ink was adopted for the interconnections. The Seebeck coefficient, S, of the screen-printed PEDOT:PSS film was measured using a custom-built setup[40] and was found to be $S = +12\ \mu V\ K^{-1}$. Additionally, the thermal conductivity, κ, and electrical conductivity, σ, of the films were characterized resulting in values of $\kappa = 0.5\ W\ m^{-1}\ K^{-1}$ and $\sigma = 37\ S\ cm^{-1}$. Detailed information can be found in the Supporting information (Figure S2, Supporting Information).

Two variants of PEDOT:PSS TEGs were fabricated, with $n = 4$ (*P4*) and $n = 8$ (*P8*) thermocouples, as shown in **Figure 2**a,b, respectively. These variants exhibit in 14 µm thick Ag and PEDOT:PSS legs. The *P4* devices were found to have an internal device resistance of $R_{TEG} = 10\ \Omega$ while the *P8* devices had an internal resistance of $R_{TEG} = 19\ \Omega$, indicating the predictable scaling of the internal resistance with the doubling of the number of thermoelements. The power output of these TEGs was characterized using a previously described measurement setup.[41] The open circuit voltage, V_{OC}, was measured as a function of the applied temperature difference, ΔT, between the bottom and the top of the device, including the substrate. Small-to-moderate temperature gradients, ranging from $\Delta T = 5$ K to $\Delta T = 25$ K, were selected to align with realistic conditions for an IoT scenario. Figure 2c and d show the V_{OC} at varying temperature gradients for both the *P4* and *P8* TEGs. As anticipated, V_{OC} exhibits a linear dependence with respect to ΔT, according to:[42]

$$V_{OC} \propto n \cdot S_{pn} \cdot \Delta T \tag{1}$$

where the S_{pn} is the difference of Seebeck coefficients of the thermoelectric materials.

Additionally, the power output, P_{OUT}, was measured as a function of the applied load resistance, $R_{LOAD,}$ for varying ΔT values. Figure 2e,f show the output power over varying load resistances for both *P4* and *P8* TEGs. The measured power outputs exhibit an ideal behaviour with maximum power output ($P_{OUT\ MAX}$) obtained when the load resistance is matched to the internal resistance following the equation:[43]

$$P_{OUT} = (V_{OC})^2 \frac{R_{LOAD}}{(R_{TEG} + R_{LOAD})^2} \tag{2}$$

The ideal behaviour was further confirmed as the $P_{OUT\ MAX}$ (**Table 2**) obtained from the *P4* TEG is exactly half of the P_{OUT} obtained by the *P8* TEG for every ΔT, demonstrating the appropriate scaling of the P_{OUT} of the TEGs. The reproducibility of the ideal behaviour of this new architecture has been demonstrated in at least two different devices fabricated in two separate runs (Figure S3, Supporting Information).

2.3. TEG Based on an Additive-Free Graphene Ink

Following the successful validation of the fully screen-printed architecture with PEDOT:PSS-based p-type legs, a screen-printable p-type semiconductor with improved thermoelectric performance over PEDOT:PSS was incorporated into the architecture. A recently reported additive-free graphene ink formulation,[30] not previously assessed for thermoelectric applications, was selected. In this graphene ink formulation, van der Waals interactions replace the role of the additives in overcoming the processing challenges, thereby largely preserving the electronic properties of the material.[30]

The screen-printable graphene ink demonstrated a room-temperature Seebeck coefficient of $S = 48\ \mu V\ K^{-1}$, a thermal con-

Table 2. Comparison of the $P_{OUT\ MAX}$ of the P4 TEG and the P8 TEG for varying ΔT values. The $P_{OUT\ MAX}$ of the P4 was measured at 9.3 K and 22.7 K, while the $P_{OUT\ MAX}$ of the P8 TEG was measured at 9 K and 25 K.

TEG	$P_{OUT\ MAX}$ ΔT 9 K [nW]	$P_{OUT\ MAX}$ ΔT 22 – 25 K [nW]
P4	0.15	0.93
P8	0.24	1.75

© 2024 The Authors. Advanced Materials Technologies published by Wiley-VCH GmbH

2365709x, 0, Downloaded from https://onlinelibrary.wiley.com/doi/10.1002/admt.202302058 by Karlsruher Institut F., Wiley Online Library on [10/04/2024]. See the Terms and Conditions (https://onlinelibrary.wiley.com/terms-and-conditions) on Wiley Online Library for rules of use; OA articles are governed by the applicable Creative Commons License

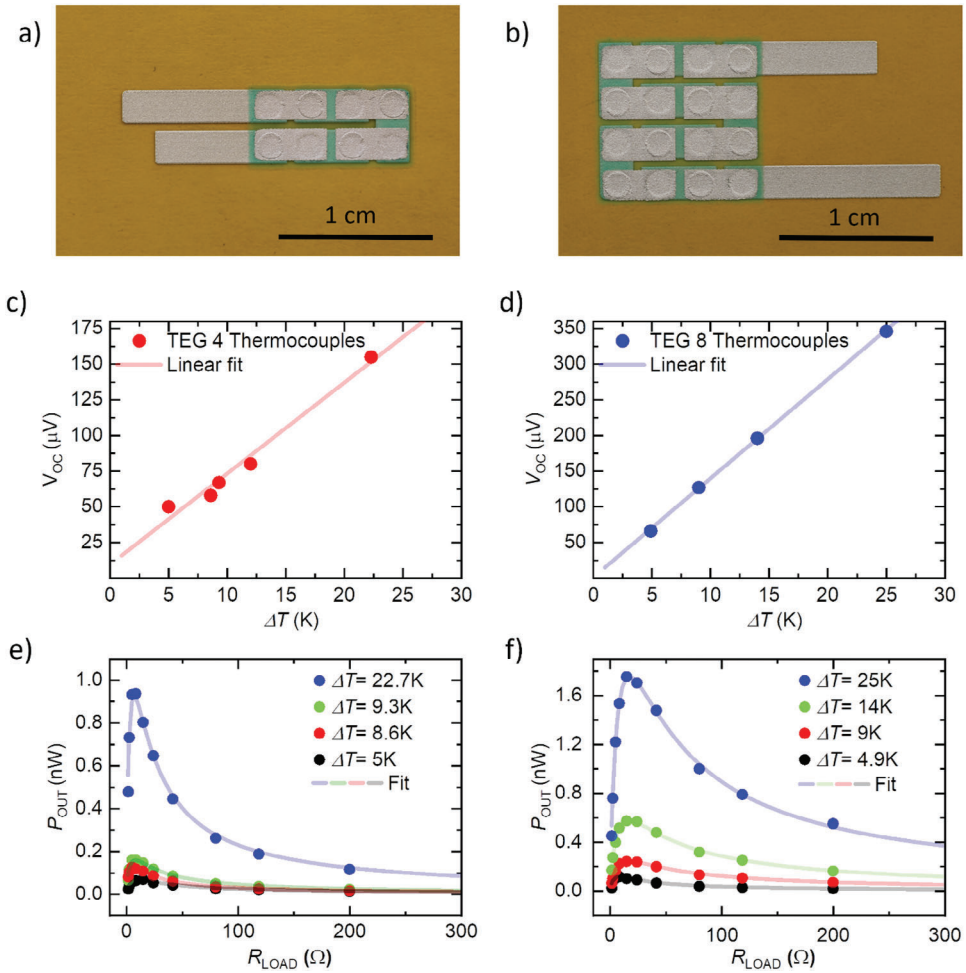

Figure 2. a) Photograph of the P4 TEG. b) Photograph of the P8 TEG. Open circuit voltage of the c) P4 TEG and of the d) P8 TEG as a function of the ΔT. Power output of the e) P4 TEG and of the f) P8 TEG as a function of the resistive load for different ΔT. The fittings (lines) in panels e) and f) are rational polynomials.

ductivity of $\kappa = 0.3$ W m^{-1} K^{-1} and an electrical conductivity of $\sigma = 41$ S cm^{-1}. Comprehensive details can be found in the Supporting information (Figures S4,S5, and S6, Supporting Information). To compare the overall thermoelectric properties of the screen-printed graphene films to the screen-printed PEDOT:PSS films, the thermoelectric figure of merit, zT, can be used, defined as:

$$zT = \frac{S\sigma^2 T}{\kappa} \quad (3)$$

where S is the Seebeck coefficient, σ is the electrical conductivity, T is the absolute temperature, and κ is the thermal conductivity. The graphene films exhibited a $zT = 8\times10^{-3}$, versus $zT = 3\times10^{-4}$ for the PEDOT:PSS screen-printed films.

A 1×1 cm^2 TEG consisting of 8 thermocouples and mirroring the architecture of the PEDOT:PSS device (Figure 2b), but with 9 μm thick graphene legs, was fabricated. The 8 thermocouples device (*G8*) was found to have an internal resistance of 14 Ω. The V_{OC} as a function of ΔT, and P_{OUT} as a function of R_{LOAD} are reported in **Figure** 3a,b, respectively. In both cases, the data recorded exhibit an ideal behaviour, in alignment with Equation (1) and (2). This ideal and reproducible behaviour underscores the consistency of the performance of the additive-free graphene ink and the screen-printing fabrication method.

The device demonstrated a maximum power output of 15 nW at $\Delta T = 29.5$ K, establishing a new benchmark among fully printed organic TEGs for normalized power output (1.7×10^{-5} μW cm^{-2} K^{-2}), which considers the output power as a function of the square of the applied ΔT and the area of the TEG (Figure S7, Supporting Information).[38] The use of additive-free graphene significantly enhanced the power output of the device, exhibiting a 5.5-fold increase at $\Delta T = 25$ K compared to the PEDOT:PSS-based device (Figure 3c).

Additionally, the power output of the TEGs per gram was evaluated, a crucial factor in applications emphasizing portability, such as wearable electronics. The *8G* monolithic device not only proved to be remarkably lightweight, achieving an estimated power output of 1 μW g^{-1}, including the substrate, but also demonstrated a high level of flexibility, an essential characteristic in applications where conformability and durability are required. The internal resistance of the device was observed to

© 2024 The Authors. Advanced Materials Technologies published by Wiley-VCH GmbH

2365709x, 0, Downloaded from https://onlinelibrary.wiley.com/doi/10.1002/admt.202302058 by Karlsruher Institut F., Wiley Online Library on [10/04/2024]. See the Terms and Conditions (https://onlinelibrary.wiley.com/terms-and-conditions) on Wiley Online Library for rules of use; OA articles are governed by the applicable Creative Commons License

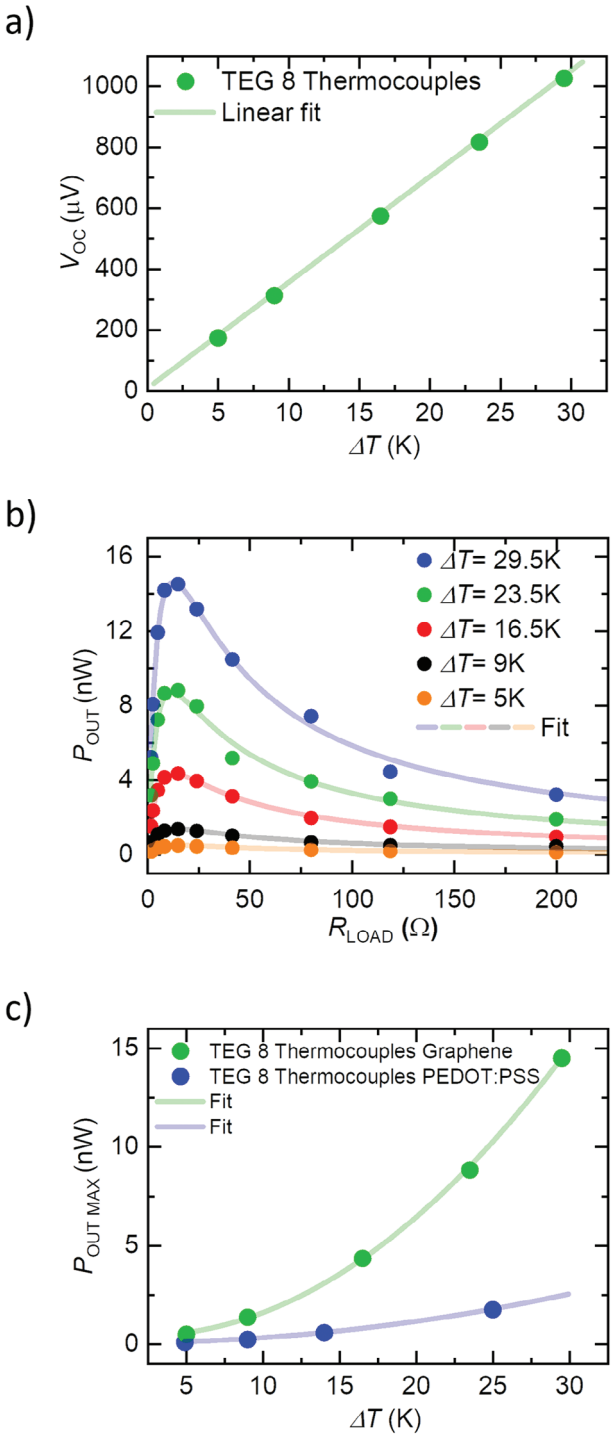

Figure 3. a) V_{OC} of the G8 TEG as a function of the ΔT (measure green dots and linear fittings). b) P_{OUT} of the G8 TEG as a function of the resistive load for different ΔT. The fittings (lines, Fit) in the graph are rational polynomials. c) Comparison between the maximum Pout of the 8G TEG (green, dots) and the maximum P_{OUT} of the P8 TEG (blue dots), as a function of the ΔT. The fittings (lines, Fit) in the graph are exponential.

remain constant even when rolled into a cylinder with a bending radius of 1 cm (Figure S8, Supporting Information).

2.4. Predictability of TEGs Performance through Finite-Element Method Simulations

The predictability of the performance of the TEGs, critical for future scaling and engineering design, was assessed using finite-element method simulations based on COMSOL Multiphysics (for more details see Note S1, Figure S9, Supporting Information). The open circuit voltages of the PEDOT:PSS-based TEGs and the additive-free graphene-based devices were simulated using nominal material parameters as input. Simulation results closely match the experimental values, as illustrated in **Figure 4** (simulation details of the *P4* device are available in the Supporting Information, Figure S10, Supporting Information).

The simulations for the V_{OC} were carried out with nominal thicknesses of 14 μm and 9 μm for PEDOT:PSS and graphene, respectively (black dots in Figure 4). However, analyzing the surface profiles of the materials, it is observed that the two printed materials have different surface roughness. Considering the increased complexity associated with simulations involving roughness an approximation is made by evaluating the effective thickness subtracting half of the average peak-to-valley height (*Rc*) from the measured nominal thickness. Considering that the profile of PEDOT:PSS has *Rc* = 0.5 μm, and the profile of the graphene has *Rc* = 2 μm, effective thicknesses of 13.75 μm and 8 μm were evaluated, respectively. The *Voc* simulations were repeated using these effective thicknesses (grey dots in Figure 4).

The measured V_{OC} generated by the PEDOT:PSS-based and the graphene-based devices show excellent agreement with the simulations, with a maximum error of 6.1% and 10.2%, respectively. Such good matching further demonstrates the possibility of reliably predicting the performance of the TEGs manufactured using the proposed fully screen-printed fabrication process.

Finite-element method simulations were employed to further investigate and identify the current limitations of thermoelectric conversion with the devices. Temperature profile along the frontal plane of the *G8* TEG at $\Delta T = 25$ °C with substrate thicknesses of 25 μm and 5 μm (**Figure 5a**) were simulated. Additionally, temperature profiles along the central axis of the graphene and the silver-based legs with varying substrate thicknesses, from 3 μm to 50 μm, are presented in Figure S11 (Supporting Information) (the temperature profiles of the *P8* TEG are shown in Figure S12, Supporting Information). These simulations demonstrate the significant influence of the substrate thickness on TEG performance, as it acts as a thermal barrier affecting the effective temperature difference, ΔT_{eff}, across the thermoelectric legs (note that the influence of the layer of parylene is demonstrated to be negligible, see Note S1, Supporting Information). In comparison, the high thermal conductivity of the silver vertical interconnections plays a reduced impact on the *Voc* since the heat transfer through different legs is essentially independent of each other (details in the Supporting Information, Figure S13).

The effect of substrate thickness on ΔT_{eff} is defined as:

$$\Delta T_{eff} = \left(\Delta T - \Delta T_{sub}\right) = \frac{V_{OC-sim}}{n\, S_{pn}} \tag{4}$$

© 2024 The Authors. Advanced Materials Technologies published by Wiley-VCH GmbH

2365709x, 0, Downloaded from https://onlinelibrary.wiley.com/doi/10.1002/admt.202302058 by Karlsruher Institut F., Wiley Online Library on [10/04/2024]. See the Terms and Conditions (https://onlinelibrary.wiley.com/terms-and-conditions) on Wiley Online Library for rules of use; OA articles are governed by the applicable Creative Commons License

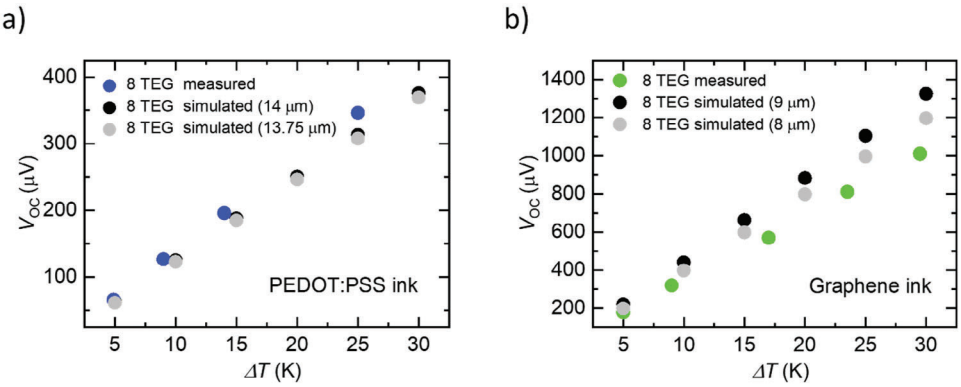

Figure 4. a) Comparison between the V_{OC} of the P8 TEG as a function of ΔT (blue dot) and simulated with a leg thickness of 14 µm (black dot), and a leg thickness of 13.75 µm (grey dot). b) Comparison between the V_{OC} of the 8G TEG as a function of the ΔT measured (green dot) and simulated with a leg thickness of 9 µm (black dot), and a leg thickness of 8 µm (grey dot).

where ΔT_{sub} is the temperature drop across the substrate, and the $V_{OC\text{-}sim}$ is the open circuit voltage obtained from the simulations. Various combinations of substrate and leg thicknesses were simulated (Figure 5b), revealing that increasing the leg thickness reduces the impact of the substrate on ΔT_{eff}. This effect tends to be more pronounced with thinner substrates and thicker legs, where ΔT_{eff} approaches ΔT. Consequently, reducing substrate thickness emerges as a viable strategy to increase the TEG performance.

Another approach to increase the ΔT_{eff} is to utilize substrate material with higher thermal conductivity. For instance, using a substrate with a thickness of 25 µm and thermal conductivity of 0.8 W m^{-1} K^{-1}[44] could yield a power output 15 times higher than that obtained with the Kapton substrates used in the presented devices. In the case of the presented 1×1 cm^2 graphene device, the power output would reach 250 nW at ΔT = 29.5 K. The power generated by the device also increases as the thickness of the active material increases, since the V_{OC} rises, until the leg resistance becomes dominant, and the power begins to decrease. However, this effect is only observed at thicknesses above 50 µm, a range not easily achievable with screen printing, as shown in Figure S14 of the Supporting Information.

2.5. Scaling up of Printed TEGs

To demonstrate the scalability of the TEGs realized according to the presented fabrication process, additive-free graphene based-TEGs were fabricated, consisting of n = 800 thermocouples with leg thicknesses of 10 µm and 20 µm, each 10 × 10 cm^2 in size (*G800*, Figure S15, Supporting Information). For comparison, new TEGs with 8 thermocouples were also screen-printed with identical leg thicknesses (*G8* TEG 10 µm, *G8* TEG 20 µm). As anticipated, the internal resistances of the *G800* TEGs increased linearly with both the number of thermocouples and the thickness of the legs, as shown in **Figure 6**. Specifically, the *G8* TEG 10 µm had an internal resistance of 3.4 Ω and the *G8* TEG 20 µm had an internal resistance of 7.5 Ω, while the *G800* TEG 10 µm and *G800* TEG 20 µm exhibited internal resistances of 325 Ω and 735 Ω, respectively. This resulted in a percent error of 5% and 2% with respect to the values obtained by multiplying the resistances values of the G8 TEG 10 µm and G8 TEG 20 µm by a factor of 100, thus demonstrating a high degree of consistency as the devices are scaled.

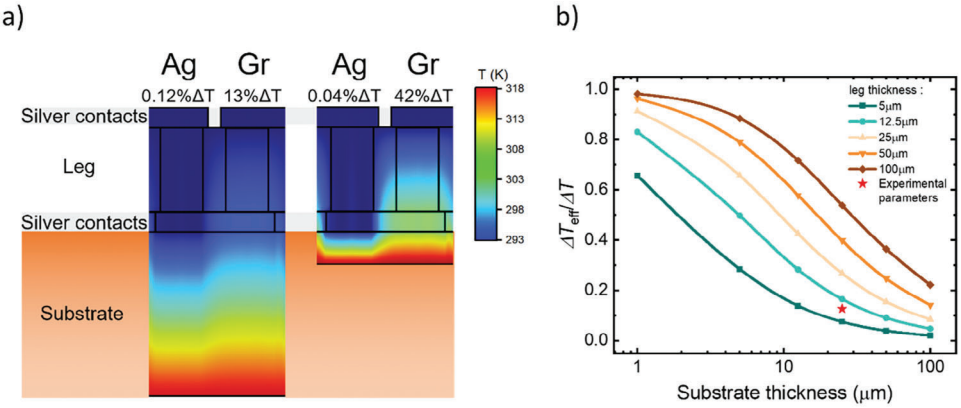

Figure 5. a) Temperature distribution along the cross-section of 2 graphene-based devices with a substrate thickness of 25 µm (left) and 5 µm (right). The temperature drops along the silver and graphene legs are independent of each other. On top of the leg is reported the ΔT_{eff} drop across the leg. b) Simulated ΔT_{eff} difference for different combinations of additive-free graphene leg thicknesses and substrate thicknesses. The ΔT_{eff} is normalized to the ΔT applied between the top and the bottom of the device, including the substrate.

© 2024 The Authors. Advanced Materials Technologies published by Wiley-VCH GmbH

2365709x, 0, Downloaded from https://onlinelibrary.wiley.com/doi/10.1002/admt.202302058 by Karlsruher Institut F. , Wiley Online Library on [10/04/2024]. See the Terms and Conditions (https://onlinelibrary.wiley.com/terms-and-conditions) on Wiley Online Library for rules of use; OA articles are governed by the applicable Creative Commons License

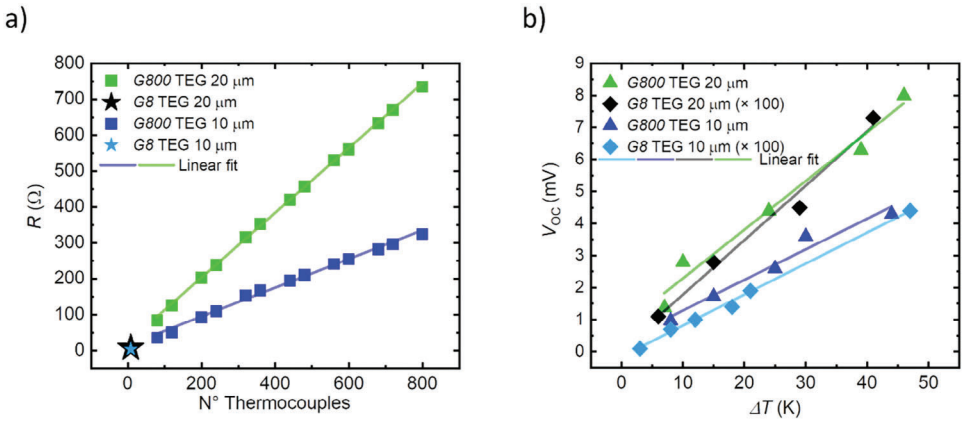

Figure 6. a) Internal resistance of the G800 TEG 10 µm (blue squares, blue linear fit) and the G800 TEG 20 µm (green squares, green linear fit) as a function of the number of thermocouples, and internal resistance of the G8 TEG 10 µm (light blue star) and of the G8 TEG 20 µm (black star)b) Comparison between the V_{OC} of the G800 TEG 10 µm (blue triangle, blue linear fit), the V_{OC} of the G8 TEG 10 µm (light blue rhombus, light blue linear fit) multiplied by a factor 100, the V_{OC} of the G800 TEG 20 µm (green triangle, green linear fit), and the V_{OC} of the G8 TEG 20 µm (black rhombus, black linear fit) multiplied by a factor 100 as a function of ΔT.

The V_{OC} of the *G800* TEG 10 µm and the *G800* TEG 20 µm devices were measured as a function of ΔT (Figure 6b). Here too, a linear dependence between V_{OC} and ΔT was observed. Notably, the V_{OC} of the *G800* TEG 10 µm was half that of the *G800* TEG 20 µm at the same ΔT, consistent with predictions. This is because the thickness of the legs of the former is half that of the latter, consequently halving the ΔT_{eff} affecting the device. For example, at $\Delta T = 40$ K, the V_{OC} values were measured to be 3.9 mV and 6.9 mV, respectively.

The *G8* TEG 10 µm, and the *G8* TEG 20 µm were similarly characterized to verify the process scalability (Figure 6b). The V_{OC} of *G8* TEGs proved to be 100 times lower than those produced by the *G800* TEGs, at the same ΔT. At a $\Delta T = 40$ K, the V_{OC} of the *G8* TEG 10 µm multiplied by a factor of 100 was 3.7 mV, with an error of 5.1% compared to the V_{OC} of the *G800* TEG 10 µm, while the V_{OC} of the *G8* TEG 20 µm multiplied by a factor of 100 was 6.8 mV, with a percent error of 1.5% compared to the V_{OC} of the *G800* TEG 10 µm, showcasing remarkable scalability.

The scalability was also demonstrated in the case of the maximum power output provided by the devices. In detail, the $P_{OUT\,MAX}$ of the *G800* TEG 20 µm device was 16 nW, 106 times the $P_{OUT\,MAX}$ of the *G8* TEG 20 µm device (0.15 nW). In the case of the *G800* TEG 10 µm and the *G8* TEG 10 µm the ratio between the two powers was 102, as the $P_{OUT\,MAX}$ were 10.2 nW and 0.1 nW, respectively.

The scalability and the reproducibility of the structure were demonstrated over two months in at least two different devices fabricated during two separate printing runs (Figures S16 and S17, Supporting Information).

These findings indicate that the presented fabrication process is highly scalable to tens of cm^2-areas. Using the same screen printer and the same screen typology, it is possible to easily produce the same devices with an area up to m^2. This offers significant opportunities for scaling as well as ample parallelization in the fabrication of multiple smaller-area TEGs.

3. Conclusion

This work has established a fabrication method for producing robust, large area, fully printed vertical organic TEGs. Utilizing a straightforward, cost-effective process, it is possible to design and fabricate flexible, lightweight TEGs scalable up to m^2 dimensions. These TEGs exhibit consistent performance aligning with simulated results based on the figures of merit of the constituent materials and maintain stability over extended months.

The TEG structure was first validated with a widely used p-type thermoelectric material, PEDOT:PSS, and a conductive silver ink, producing vertical TEGs consisting of 4 or 8 thermocouples with an area of 0.5×1 cm^2 or 1×1 cm^2, respectively.

Upon validating the reliability of the fabrication method, an 8-thermocouple TEG incorporating additive-free graphene as a p-type leg was realized. This flexible, lightweight additive-free graphene-based device achieved a significant maximum normalized power output of 1.7×10^{-5} µW cm^{-2} K^{-2}, setting a new benchmark among the fully printed organic TEGs.

However, opportunities for further enhancing the power density exist. For example, using a thinner substrate or one with higher thermal conductivity, such as employing a metal foil with a passivation layer on top, could lead to a notable increase in ΔT_{eff} across the thermoelectric legs. Moreover, the TEGs currently employ short-circuited n-type legs using silver ink due to the absence of a suitable n-type material. Therefore, the introduction of an organic, screen-printable n-type ink with performance matching the additive-free graphene would potentially double the maximum power output of a TEG fabricated using the same methodology. Additionally, the versatility of the fabrication process enables the use of any screen-printable ink, including inorganic materials known for their superior thermoelectric performance. For instance, a 1×1 cm^2 TEG with legs 14 µm thick on a 25 µm thick Kapton foil using the n-type material β-Ag_2Se[45] and the p-type material $Bi_{0.5}Sb_{1.5}Te_3$[46] could theoretically generate a power output of 10 µW at $\Delta T = 30$ K, sufficient to power low-power electronic devices or sensors.[47] Furthermore, the ability to

© 2024 The Authors. Advanced Materials Technologies published by Wiley-VCH GmbH

2365709x, 0, Downloaded from https://onlinelibrary.wiley.com/doi/10.1002/admt.202302058 by Karlsruher Institut F., Wiley Online Library on [10/04/2024]. See the Terms and Conditions (https://onlinelibrary.wiley.com/terms-and-conditions) on Wiley Online Library for rules of use; OA articles are governed by the applicable Creative Commons License

manufacture TEGs with 800 thermocouples has been demonstrated, opening up the possibility to significantly increase the power output.

In summary, the versatility of the proposed TEG architecture and fabrication process has been demonstrated with two different active inks and three configurations, incorporating up to 800 integrated thermoelements, providing evidence of the predictable customization of the device, with respect to size, materials, and power output to fit the intended application. The approach enables the engineering of TEGs that, by leveraging enhanced thermal coupling and exploiting next-generation thermoelectric inks, could meet the power needs of various distributed sensors and IoT devices operating under modest thermal gradients. This development offers a promising outlook in terms of sustainable energy harvesting.

4. Experimental Section

Screen Printable Inks: The p-type CleviousTM SV4 PEDOT:PSS was a commercial formulation supplied by Heraeus. The Ag ink (LOCTITE® ECI 1010 E&C) was purchased from Sigma–Aldrich. The Bectron DP 8446 insulator was purchased from Elantas. The additive-free graphene ink (2 vol.% pristine graphene in Terpineol) was prepared according to the procedure presented in the article.[30]

Printing Process: All the devices were screen printed on a flexible Kapton substrate, 25 µm thick, provided by DuPont Teijin Films. The devices were printed using the industrial Thieme 3010S Vision screen-print machine. All the layers were screen-printed at room temperature. After printing the silver layers (the bottom contact, the silver leg, and the top contact) the samples were annealed for 60 minutes at 90 °C in an oven. After printing the graphene leg and the PEDOT:PSS leg the devices were annealed at 100 degrees for 15 minutes on a hot plate, while after printing the insulator the samples were cured with the UV light for 10 seconds. At last, to electrically insulate the devices was used a thin layer of parylene (1 µm) deposited using the commercially available SCS PDS 2010 Labcoter® 3.

TEG Characterizations: It was worth noting that the measurement setup used to measure the devices presented in the section Validation of the TEG architecture and fabrication process and TEG based on an additive-free graphene ink and the one used to characterize the devices presented in the section Scaling up of printed TEGs were different.

The first one was the setup presented in the article,[41] which allowed voltage and power measurements under vacuum in a steady state mode. After setting the temperature of the two copper blocks using the water-based cooling system and the heater-based heating system, the two temperatures reached equilibrium and stabilized at a certain value, depending on the thickness of the device and its thermal mass. The V_{OC} reported were measured 5 minutes after reaching the equilibrium. In the second case, a simple hot press with temperature-controlled plates was used to characterize the *G800* 10 µm, *G800* 20 µm, *G8* 10 µm and *G8* 20 µm TEGs by varying the ΔT between the plates and measuring the V_{OC}. In addition, in the second case, the devices were not passivated with the parylene layer, but a passivation paper was used for electrical insulation, reducing the ΔT_{eff}. However, if the devices were considered measured using the same methods, the performance was perfectly scalable in all the cases studied.[41]

The bending measurements were made using cylinders with different diameters, and the inner resistances were measured with a Keithley 2010 multimeter.

Supporting Information

Supporting Information is available from the Wiley Online Library or from the author.

Acknowledgements

This project has received funding from the European Union's Horizon 2020 research and innovation program under the Marie Skłodowska-Curie grant agreement No 955837 – HORATES.

Open access funding enabled and organized by Projekt DEAL.

Conflict of Interest

The authors declare no conflict of interest.

Data Availability Statement

The data that support the findings of this study are available from the corresponding author upon reasonable request.

Keywords

flexible electronics, scalable device, screen printing, thermoelectric generator (TEG)

Received: November 30, 2023
Revised: February 18, 2024
Published online:

[1] R. Kandpal, R. Singh, *ECS Trans.* **2022**, *107*, 8133.
[2] T. Z. Ang, M. Salem, M. Kamarol, H. S. Das, M. A. Nazari, N. Prabaharan, *Energy Strat. Rev.* **2022**, *43*, 100939.
[3] H. Rahmani, D. Shetty, M. Wagih, Y. Ghasempour, V. Palazzi, N. B. Carvalho, R. Correia, A. Costanzo, D. Vital, F. Alimenti, J. Kettle, D. Masotti, P. Mezzanotte, L. Roselli, J. Grosinger, *IEEE J. Microwaves* **2023**, *3*, 237.
[4] M. A. Jamshed, K. Ali, Q. H. Abbasi, M. A. Imran, M. Ur-Rehman, *IEEE Sens. J.* **2022**, *22*, 5482.
[5] S. Sharma, V. K. Verma, *Wirel Pers. Commun.* **2022**, *124*, 2735.
[6] J. Chen, K. Hu, Q. Wang, Y. Sun, Z. Shi, S. He, *IEEE Internet Things J.* **2017**, *4*, 2309.
[7] C. Forman, I. K. Muritala, R. Pardemann, B. Meyer, *Renew. Sustain. Energy Rev.* **2016**, *57*, 1568.
[8] S. M. Pourkiaei, M. H. Ahmadi, M. Sadeghzadeh, S. Moosavi, F. Pourfayaz, L. Chen, M. A. Pour Yazdi, R. Kumar, *Energy* **2019**, *186*, 115849.
[9] X. Chen, W. Dai, T. Wu, W. Luo, J. Yang, W. Jiang, L. Wang, *Coatings* **2018**, *8*, 244.
[10] J. P. Heremans, M. S. Dresselhaus, L. E. Bell, D. T. Morelli, *Nat. Nanotechnol.* **2013**, *8*, 471.
[11] T. J. Hendricks, S. Yee, S. LeBlanc, *J. Electron. Mater.* **2016**, *45*, 1751.
[12] M. Jaishankar, T. Tseten, N. Anbalagan, B. B. Mathew, K. N. Beeregowda, *Interdiscip. Toxicol.* **2014**, *7*, 60.
[13] F. N. Gunnar, B. A. Fowler, Monica Nordberg, Handbook on the Toxicology of Metals, **2015**.
[14] Y. Khan, A. Thielens, S. Muin, J. Ting, C. Baumbauer, A. C. Arias, *Adv. Mater.* **2020**, *32*, 1905279.
[15] N. Pataki, P. Rossi, M. Caironi, *Appl. Phys. Lett.* **2022**, *121*, 230501.
[16] M. L. Chabinyc, W. S. Wong, A. C. Arias, S. Ready, R. A. Lujan, J. H. Daniel, B. Krusor, R. B. Apte, A. Salleo, R. A. Street, *Proc. IEEE* **2005**, *93*, 1491.
[17] R. Parashkov, E. Becker, T. Riedl, H. H. Johannes, W. Kowalsky, *Proc. IEEE* **2005**, *93*, 1321.
[18] M. Shakeel, K. Rehman, S. Ahmad, M. Amin, N. Iqbal, A. Khan, *Renew. Energy* **2021**, *167*, 853.

© 2024 The Authors. Advanced Materials Technologies published by Wiley-VCH GmbH

2365709x, 0, Downloaded from https://onlinelibrary.wiley.com/doi/10.1002/admt.202302058 by Karlsruher Institut F., Wiley Online Library on [10/04/2024]. See the Terms and Conditions (https://onlinelibrary.wiley.com/terms-and-conditions) on Wiley Online Library for rules of use; OA articles are governed by the applicable Creative Commons License

[19] M. Massetti, S. Bonfadini, D. Nava, M. Butti, L. Criante, G. Lanzani, L. Qiu, J. C. Hummelen, J. Liu, L. J. A. Koster, M. Caironi, *Nano Energy* **2020**, *75*, 104983.
[20] C. T. Hong, Y. H. Kang, J. Ryu, S. Y. Cho, K. S. Jang, *J. Mater. Chem. A Mater.* **2015**, *3*, 21428.
[21] Q. Wei, M. Mukaida, K. Kirihara, Y. Naitoh, T. Ishida, *RSC Adv.* **2014**, *4*, 28802.
[22] F. Jiao, C. A. Di, Y. Sun, P. Sheng, W. Xu, D. Zhu, *Philos. Trans. R. Soc., A* **2014**, *372*, 20130008.
[23] C. K. Mytafides, L. Tzounis, G. Karalis, P. Formanek, A. S. Paipetis, *ACS Appl. Mater. Interfaces* **2021**, *13*, 11151.
[24] B. Dörling, J. D. Ryan, J. D. Craddock, A. Sorrentino, A. El Basaty, A. Gomez, M. Garriga, E. Pereiro, J. E. Anthony, M. C. Weisenberger, A. R. Goñi, C. Müller, M. Campoy-Quiles, *Adv. Mater.* **2016**, *28*, 2782.
[25] C. Y. Yang, M. A. Stoeckel, T. P. Ruoko, H. Y. Wu, X. Liu, N. B. Kolhe, Z. Wu, Y. Puttisong, C. Musumeci, M. Massetti, H. Sun, K. Xu, D. Tu, W. M. Chen, H. Y. Woo, M. Fahlman, S. A. Jenekhe, M. Berggren, S. Fabiano, *Nat. Commun.* **2021**, *12*, 2354.
[26] S. Ferhat, C. Domain, J. Vidal, D. Noël, B. Ratier, B. Lucas, *Sustain. Energy Fuels* **2018**, *2*, 199.
[27] R. R. Søndergaard, M. Hösel, N. Espinosa, M. Jørgensen, F. C. Krebs, *Energy Sci. Eng.* **2013**, *1*, 81.
[28] R. Tkachov, L. Stepien, M. Greifzu, A. Kiriy, N. Kiriy, T. Schüler, T. Schmiel, E. López, F. Brückner, C. Leyens, *Coatings* **2019**, *9*, 764.
[29] H. Andersson, P. Šuly, G. Thungström, M. Engholm, R. Zhang, J. Mašlík, H. Olin, *J. Low Power Electron. Appl.* **2019**, *9*, 14.
[30] S. Abdolhosseinzadeh, C. Zhang, R. Schneider, M. Shakoorioskooie, F. Nüesch, J. Heier, *Adv. Mater.* **2022**, *34*, https://doi.org/10.1002/adma.202103660.
[31] S. Kee, M. A. Haque, D. Corzo, H. N. Alshareef, D. Baran, *Adv. Funct. Mater.* **2019**, *29*, 2103660.
[32] R. Tkachov, L. Stepien, M. Greifzu, A. Kiriy, N. Kiriy, T. Schüler, T. Schmiel, E. López, F. Brückner, C. Leyens, *Coatings* **2019**, *9*, 764.
[33] I. Dani, A. Roch, L. Stepien, C. Leyens, M. Greifzu, M. Von Lukowicz, IFIP AICT 411 – Energy Turnaround: Printing of Thermoelectric Generators, **2013**.
[34] S. Ferhat, C. Domain, J. Vidal, D. Noël, B. Ratier, B. Lucas, *Sustain. Energy Fuels* **2018**, *2*, 199.
[35] T. Juntunen, H. Jussila, M. Ruoho, S. Liu, G. Hu, T. Albrow-Owen, L. W. T. Ng, R. C. T. Howe, T. Hasan, Z. Sun, I. Tittonen, *Adv. Funct. Mater.* **2018**, *28*, 1800480.
[36] E. Yvenou, M. Sandroni, A. Carella, M. N. Gueye, J. Faure-Vincent, S. Pouget, R. Demadrille, J. P. Simonato, *Mater. Chem. Front.* **2020**, *4*, 2054.
[37] Q. H. Zhang, X. Y. Huang, S. Q. Bai, X. Shi, C. Uher, L. D. Chen, *Adv. Eng. Mater.* **2016**, *18*, 194.
[38] S. Masoumi, S. O'Shaughnessy, A. Pakdel, *Nano Energy* **2022**, *92*, 106774.
[39] Y. G. Lee, J. Kim, M. S. Kang, S. H. Baek, S. K. Kim, S. M. Lee, J. Lee, D. Bin Hyun, B. K. Ju, S. E. Moon, J. S. Kim, B. Kwon, *Adv. Mater. Technol.* **2017**, *2*, 1600292.
[40] D. Beretta, P. Bruno, G. Lanzani, M. Caironi, *Rev. Sci. Instrum.* **2015**, *86*, 075104.
[41] D. Beretta, M. Massetti, G. Lanzani, M. Caironi, *Rev. Sci. Instrum.* **2017**, *88*, 015103.
[42] A. Dyer, *Encyclopedia of Materials: Science and Technology*, 2nd ed., **2006**.
[43] E. F. Sawires, M. I. Eladawy, Y. I. Ismail, H. Abdelhamid, *IEEE Access* **2018**, *6*, 8123.
[44] https://www.dupont.com/electronics-industrial/kapton-mt-plus.html.
[45] M. M. Mallick, A. G. Rösch, L. Franke, A. Gall, S. Ahmad, H. Geßwein, A. Mazilkin, C. Kübel, U. Lemmer, *J. Mater. Chem. A Mater.* **2020**, *8*, 16366.
[46] M. M. Mallick, L. Franke, A. G. Rösch, S. Ahmad, H. Geßwein, Y. M. Eggeler, M. Rohde, U. Lemmer, *ACS Appl. Mater. Interfaces* **2021**, *13*, 61386.
[47] M. Shirvanimoghaddam, K. Shirvanimoghaddam, M. M. Abolhasani, M. Farhangi, V. Z. Barsari, H. Liu, M. Dohler, M. Naebe, *IEEE Access* **2019**, *7*, 94533.

© 2024 The Authors. Advanced Materials Technologies published by Wiley-VCH GmbH

2365709x, 0, Downloaded from https://onlinelibrary.wiley.com/doi/10.1002/admt.202302058 by Karlsruher Institut F., Wiley Online Library on [10/04/2024]. See the Terms and Conditions (https://onlinelibrary.wiley.com/terms-and-conditions) on Wiley Online Library for rules of use; OA articles are governed by the applicable Creative Commons License